Interface creep behavior of tensioned GFRP tendons embedded in cemented soils

C. Chen[1], S. Zhu[2], G. Zhang[3], A. M. Morsy[4], J. G. Zornberg[5] and J. Huang[6]

[1] *Professor, Key Laboratory of Building Safety and Energy Efficiency of the Ministry of Education, Hunan University, Changsha, P.R. China; College of Civil Engineering, Hunan University, Changsha, Hunan, P.R. China. Email: cfchen@hnu.edu.cn*
[2] *PhD Candidate, Key Laboratory of Building Safety and Energy Efficiency of the Ministry of Education, Hunan University, Changsha, P.R. China; College of Civil Engineering, Hunan University, Changsha, Hunan, P.R. China. Email: smzhu@hnu.edu.cn*
[3] *Assistant Professor, College of Civil Engineering, Hunan City University, Yiyang, Hunan, P.R. China. Email: gbzhang@hnu.edu.cn (corresponding author)*
[4] *Research Associate, School of Architecture, Building and Civil Engineering, Loughborough University, Leicestershire, UK; Assistant Professor, Department of Civil Engineering, Cairo University, Giza 12613, Egypt. Email: a.morsy@lboro.ac.uk*
[5] *Professor, Department of Civil, Architectural and Environmental Engineering, The University of Texas at Austin, Austin, Texas, USA. Email: zornberg@mail.utexas.edu*
[6] *Formerly Master Candidate, Key Laboratory of Building Safety and Energy Efficiency of the Ministry of Education, Hunan University, Changsha, P.R. China; College of Civil Engineering, Hunan University, Changsha, Hunan, P.R. China. Email: 453029088@qq.com*

Received 13 February 2020, accepted 18 March 2021, published 15 February 2022

ABSTRACT: This paper presents an experimental investigation and modeling of interface creep behavior of glass fiber-reinforced polymer (GRFP) tendons embedded in cemented soils. Rapid and creep pullout tests were carried out on GRFP tendons embedded in cemented soils using a specially developed pullout setup. Interface creep displacement responses for specimens with two different water–cement ratios were derived under various interface shear stress conditions. A modified Burgers model was developed to characterize the interface creep behavior by incorporating a time-dependent viscosity coefficient. This viscosity coefficient was calibrated using creep rate variation obtained experimentally. Regression fittings on a part of interface creep measurements were conducted to determine the value of the parameters of the interface creep model. Additional interface creep measurements were used to validate the applicability of the presented creep testing protocol and the effectiveness of the rheological modeling was validated.

KEYWORDS: Geosynthetics, Glass fiber-reinforced polymer, Cemented soils, Interface creep behavior, Burgers model

REFERENCE: Chen, C., Zhu, S., Zhang, G., Morsy, A. M., Zornberg, J. G. and Huang, J. (2022). Interface creep behavior of tensioned GFRP tendons embedded in cemented soils. *Geosynthetics International*, **29**, No. 3, 241–253. [https://doi.org/10.1680/jgein.21.00008]

1. INTRODUCTION

Reinforced soil-mixing technology has been increasingly used in civil engineering projects to furnish sound solutions for earth retention and ground stabilization due to their efficient construction and versatile applicability to different ground conditions. Typical types of reinforced soil-mixing structures include deep mixing walls (DMW) reinforced with formed steel sections, cement-soil piles reinforced with steel rebar cage, and soil-mixing anchors with steel reinforcement rebars (Liu *et al*. 2010; CECS 2016). The primary source of reinforcement degradation in these structures is corrosion; an issue that is particularly pronounced in coastal regions characterized by the presence of abundant corrosive soils. Fiber-reinforced polymer (FRP) materials have been used as a substitute to steel materials in the reinforcement of soil-mixing structures (Zhu *et al*. 2011; Zheng and Dai 2014a, 2014b; Sheikh and Kharal 2018; Chen *et al*. 2018b). Among fiber admixtures used with FRP materials (e.g. aramid, basalt, and carbon), glass fiber-reinforced polymer (GFRP) has been the most commonly used in civil engineering projects (e.g. reinforced concrete structures (Alves *et al*. 2011; ACI 2015; Sheikh and Kharal 2018), anchored systems (Benmokrane *et al*. 1996; Cheng *et al*. 2009; Bai *et al*. 2015; Kou *et al*. 2015; Xu and

Yin 2016), and pile foundation (Iskander *et al*. 2001; Mirmiran *et al*. 2002; Sakr *et al*. 2004; Guades *et al*. 2012; Kim and Andrawes 2016)) because of its satisfactory performance and cost efficiency.

The performance of reinforced soil-mixing structures depends on the extent of interface shear strength (i.e. bond strength) mobilization between reinforcements and their encapsulating cemented soils. In a laboratory, the bond strength is mainly determined using direct shear and/or pullout testing on element-reinforced specimens (Bakeer *et al*. 1998; Chu and Yin 2005). A direct shear test is suitable for geosynthetic reinforcement installed in a geomaterial matrix in planar layers (Liu *et al*. 2016), while a pullout test is favored over direct shear testing for its ability to model the actual working conditions of reinforced soil-mixing structures where the interface shear stress is generated axisymmetric on the skin of the rebars with circular sections. Pullout testing is more commonly adopted in practice to characterize the interface behavior of reinforcements in various types of materials, particularly for interface shear strength characterization of GFRP tendons embedded in sands (Frost and Han 1999; Zhang *et al*. 2015), concretes (Mukhtar and Faysal 2018; Zemour *et al*. 2018), and cemented soils (Chen *et al*. 2019a). Similarly, the interface shear behavior of cemented soils with other various materials (e.g. steel bar reinforcement (Chen *et al*. 2018b), rocks (Nasir and Fall 2008; Koupouli *et al*. 2016), and concrete (Jamsawang *et al*. 2008)) was also investigated.

It was reported that the mechanical properties of cemented soils and of their interfaces with reinforcements are largely influenced by several factors, such as cemented soil conditions (Consoli *et al*. 2011), cement–soil dosage, curing conditions, and reinforcement properties (Chen *et al*. 2018b, 2019a). Previous studies revealed that these influence factors correlate with the cemented soil-reinforcement interface strength. Such correlations could be obtained by pullout tests, which can characterize the cemented soil-reinforcement interface behavior. For instance, interface ultimate strengths of steel and GFRP reinforcements were found to be 40% and 51%, respectively, of the unconfined compressive strength of the encapsulating cemented soil (Chen *et al*. 2018b, 2019a).

The design life of reinforced soil-mixing structures is required to be at least one year, as specified by the China Association for Engineering Construction Standardization (CECS 2016); hence, time effect should be accounted for in designing such structures. Specifically, the interface creep behavior of reinforcement in cemented soils requires adequate understanding to predict the long-term performance of reinforced soil-mixing structures. The long-term interface characterization of anchors is commonly implemented by integrating pullout creep tests with rapid pullout tests in the same testing setup (Chen *et al*. 2016, 2018a; Gao *et al*. 2018). This facilitates identifying the rheological contribution of cemented soils and reinforcements to the interface behavior from the creep test phases. A number of researches investigated the rheological properties of reinforcements including FRP tendons (e.g. Wang *et al*. 2004; Ascione *et al*. 2012; Najafabadi *et al*. 2018), material mixtures including soils (e.g. Sun 1999; Lu *et al*. 2008) and rocks (e.g. Tan and Kang 1980; Liu *et al*. 2018; Mansouri and Ajalloeian 2018), which provide adequate understanding of the creep behavior of individual components of reinforced soil-mixing structures. In addition, pullout creep experimentation on soil nailing and ground anchors were extensively carried out to characterize the influence of various factors including physical properties of soil, grouting pressure, and in-service environment on the interface creep behavior between grouts and soils (e.g. Bai *et al*. 2015; Chen *et al*. 2016, 2018a 2019b, 2019c; Gao *et al*. 2018). Based on the interpretations of pullout test data, interface creep behavior could be modeled using rheological element models (Chen *et al*. 2016), and empirical models based on various algorithms including radical basis function neural network-based creep model (e.g. Gao *et al*. 2018) and factional derivative-based creep model (e.g. Chen *et al*. 2018a). Because both the construction methods and materials of reinforced soil-mixing structures are quite different from that of grouted anchors, it is particularly necessary to investigate the long-term performance of these structures. As a critical governing factor for work performance of reinforced soil-mixing structures, the interface creep behavior of reinforcement (typically exemplified by GFRP tendons) in cemented soils has not been studied either by experimental testing or theoretical modeling.

This paper presents a research study aimed at characterizing the interface creep of GFRP tendons embedded in cemented soils. The study involved interface experimental characterization and rheological modeling. Pullout tests were conducted on element GRFP tendons embedded in cemented soils with varying cement contents (i.e. water/cement ratios). The pullout testing setup used in this study was developed by Chen *et al*. (2016) with some modifications to accommodate creep tests (Chen *et al*. 2016, 2018a 2019c; Gao *et al*. 2018). A stepwise loading strategy was adopted in the creep tests to develop a time history of pullout displacements for each loading step. A conventional Burgers model was modified to characterize the interface creep behavior based on the collected experimental data.

2. MATERIALS PROPERTIES

Reinforced cemented soil specimens comprised three materials: soil, cement, and GFRP tendons. The soil samples used in this study were collected from a floodplain along the Xiangjiang River in Changsha city, China. Fig. A1 in the supplemental material to this paper shows the location where the soil samples were collected. Figure 1 shows the particle size distribution of this soil, which was determined by sieve analysis and hydrometer testing. The soil consists of approximately 36% sand, 62% silt, and 2% clay. The reinforcement used in this study was a GFRP tendon 23 cm in length and 16 mm in diameter. The loaded end of the GFRP tendon was affixed with epoxy to two locked nuts, as shown in Fig. A2, which

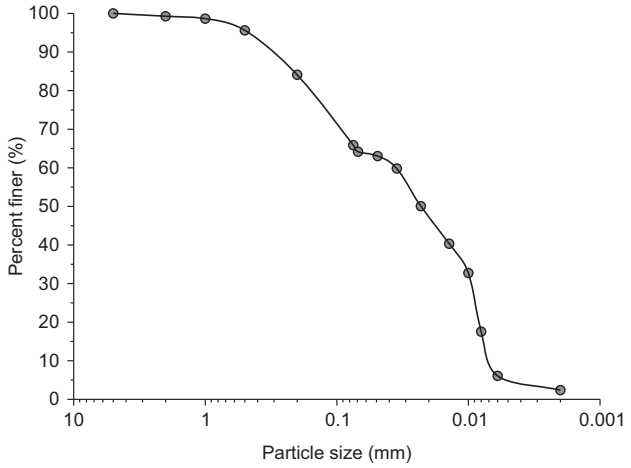

Figure 1. Particle size distribution curve of the tested soil sample

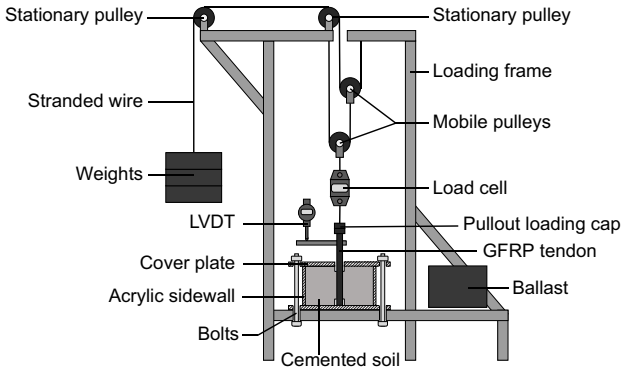

Figure 2. Schematic of creep pullout setup used in this test

served as a pullout loading cap. Ordinary Portland cement (P.O. 42.5) was used in this study to produce the cemented soil samples. The properties of the materials used in this study are listed in Table 1.

3. TESTING DEVICES AND PROCEDURE

3.1. Creep pullout test setup

The creep pullout test setup used in this study was previously used for element soil nail and ground anchor tests (Chen *et al*. 2016, 2018a 2019c; Gao *et al*. 2018). The configuration of the creep pullout test setup is illustrated in Figures 2 and A3. The setup consists of three main components: (1) a loading frame, which served as load transfer platform and reaction (stabilized ballast); (2) a pulley system, which served in conveyance of the applied load to the GFRP tendon; and (3) instrumentation, which included a load cell to monitor the pullout load and a linear variable differential transformer (LVDT) to monitor the pullout displacement. The pulley system was used to change the direction of the applied load as well as to amplify its magnitude up to 4 kN. The reinforced specimen was placed in a pullout cell, which was fully constrained in the test setup. The pullout cell was fixed to the base of the frame and the upward movement of the specimen was constrained by a cover plate, which was securely fastened to the frame base using four screw-tight bolts, as shown in Figures 2 and A3. The cover plate was designed with a center aperture 24 mm in diameter, which was carefully designed to ensure the vertical movement of the reinforcing tendon out of the pullout cell without compromising the constraint on the cemented soil sample. The reinforcing tendon was axially connected to the load cell with a split cylindrical connection, as shown in Fig. A4. The connection consisted of two threaded halves that assemble with two locking rings to form a cylinder capable of securing the pullout loading cap of the reinforcing tendon.

Table 1. Materials properties

	Property	Unit	Value/ Description
Soil	Natural water content (w)	%	30–70
	Bulk density (ρ)	Mg/m^3	1.75
	Void ratio (e)	—	1.42
	Specific gravity (G_s)	—	2.70
	Liquid limit (w_l)	%	46.8
	Plastic limit (w_p)	%	22.0
	Plasticity index (I_p)	%	24.8
	Coefficient of uniformity (C_u)	—	5.0
	Coefficient of curvature (C_z)	—	0.648
	Undrained shear strength (c_u)	kPa	20.4
GFRP tendon	Nominal diameter (d_n)	mm	16
	Rib height (R_h)	mm	1.5 ± 0.4
	Rib spacing (R_s)	mm	10 ± 0.5
	Tensile strength (σ_b)	MPa	466
	Elasticity modulus (E)	GPa	40
Cement	Type		P.O. 42.5
	Compressive strength	MPa	≥42.5 (28-day)

3.2. Testing procedure

The procedure of the creep pullout tests involved four steps: soil processing, cemented soil mixing, pullout specimen preparation, and pullout load application. This section presents each step in the test procedure.

3.2.1. *Soil processing*

Natural soil samples were air-dried in a laboratory to maintain the organic component. After being cleaned of foreign materials, soil samples were mechanically pulverized by a steel roller. To attain reasonable uniformity of soil samples suitable for mixing with cements, soil particles passing through a 5-mm sieve were reserved. Soil samples were conditioned with a water content of 2.1% in sealed plastic bags (JGJ/T 2011).

3.2.2. *Cemented soil mixing*

Water content (C_w) and cement content (C_c) were used to characterize the dosage of cemented soils, as defined in Chen *et al*. (2018b). The water content (C_w) is the ratio of water mass to dry soil mass; while, the cement content (C_c) is the ratio of cement mass to the summation of both

dry soil mass and water mass. Two groups of cemented soil specimens were prepared and tested with different combinations of water and cement contents, as listed in Table 2.

To control the water and cement contents in mixing, the calculated quantities of soil samples and cements were weighed and mixed uniformly in an agitator for 60 s. Then distilled water was added to the agitator and mixing continued for 480 s. This two-phase mixing process was aimed at homogenizing the cemented soil specimens.

3.2.3. *Pullout specimen preparation*

The creep behavior of the reinforced soil-mixing structure depends on the incorporation of the respective time-dependent performance of all components constituting the structure (Chen *et al.* 2016, 2018b 2019a, 2019b; Zhang *et al.* 2020). The anchors in short bond length could be employed to characterize the interface constitutive relationship due to a uniform distribution of the interface shear stress over the entire bond length (Benmokrane *et al.* 1995; Chen *et al.* 2016; Zhang *et al.* 2020). Hence, the pullout cell designed by Chen *et al.* (2018b), shown in Figure 3, was used in preparing the pullout specimens. The cell is 120 mm in height and 192 mm in diameter, and comprises a cover plate, an acrylic sidewall, and a base plate. The cover and base plates were mounted tightly with the acrylic sidewall, ensuring proper sealant at the intersections. Both plates were tailored with a center tube 20 mm in length and 19 mm in diameter to centralize the GFRP tendon embedded in the cemented soils, as shown in Figure 3. Using this pullout cell renders a tendon bond length of 80 mm, which is five times the tendon's nominal diameter. The ratio between the diameter of the reinforced cemented soil specimen (192 mm) and the diameter of the GFRP tendon (16 mm) is 12, which is deemed adequate to minimize the boundary effect of the cell on the specimen (Cooke *et al.* 1979). Therefore, the testing results can be reasonably used to reflect the actual interface creep behavior between GFRP tendons and cemented soils.

Table 2. Water and cement contents for the experimental specimen groups

Test group	C_w	C_c
Group 1	0.80	0.24
Group 2	0.80	0.12

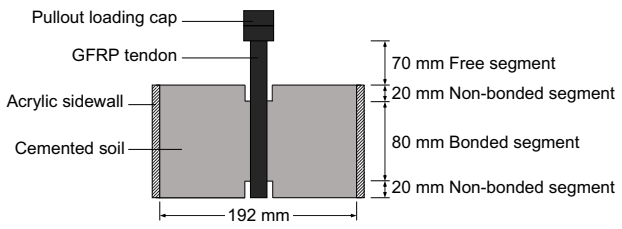

Figure 3. Schematic of the pullout specimen

The preparation of pullout specimens using a pullout cell is illustrated in Fig. A5. All surfaces of the pullout cell contacting cemented soils were coated with petroleum jelly to minimize boundary friction. The center tube of the base plate and the center aperture of the cover plate were used to centralize the GFRP tendon vertically in the cemented soil specimen. The pullout specimen with tendon and cemented soils installed was vibrated on a shaking table to ensure uniform density and to minimize bubbles entrapped inside the cemented soils. Pullout specimens were then cured in sealed bags in two phases: 48-h early phase with cover and base plates; 180-day primary phase with cover and base plate detached. Curing time affects the interface creep behavior due to the strength growth of cemented soils over time, but the increasing rate of strength of cemented soils tends to be slight once the curing time exceeds 90 days (Chen *et al.* 2018b, 2020). Therefore, for a curing age of 180 days, the strength is almost constant throughout the creep testing, which allows for an unbiased comparison of test results, and in turn allows for representative modeling of interface creep behavior. The procedure of the pullout specimen preparation is schematically shown in Fig. A5. Note that two specimens were prepared for each testing group: one used in a rapid pullout test to determine the ultimate interface bond strength (UBS) and the other used in a creep pullout test to determine the long-term interface bond strength.

3.2.4. *Pullout load application*

After cemented soil specimens have completed curing, rapid pullout tests were carried out using a frictional performance testing system (FPTS) developed by the authors (Chen *et al.* 2014, 2015).

Two loading methods are commonly used in creep tests: (1) the respective loading method, in which every loading level is applied to an exclusive specimen (i.e. each specimen is tested at one load level) (Behbahani *et al.* 2016; Mansouri and Ajalloeian 2018); and (2) the stepwise loading method, in which all loading levels are consecutively applied to the same specimen (i.e. each specimen is tested at multiple load levels) (Tan and Kang 1980; Sun 1999; Shina *et al.* 2005; Lu *et al.* 2008; Chen *et al.* 2016, 2018a 2019c; Gao *et al.* 2018; Liu *et al.* 2018). A primary advantage of the stepwise loading method over the respective loading method is that the former eliminates the possible inconsistencies among different specimens. The results can be obtained adequately from a constant specimen by transforming n loading steps on the same specimen equivalently into n one-step loadings with a respective loading level on n different specimens (Tan and Kang 1980). Hence, the stepwise loading was adopted in the creep pullout tests carried out as part of this study. The stepwise loading scheme was developed to ensure that the maximum shear stress applied to the tendon-cemented soil interface is less than the UBS, as listed in Table 3. The stepwise loading scheme for the two pullout specimens used in the creep pullout test was presented in Table 3. For simplicity, Specimen in Group 1 and Specimen in Group 2

Table 3. Loading scheme used in creep pullout test

Testing specimen	Items	Loading level of creep test								UBS
		1	2	3	4	5	6	7	8	
Specimen in Group 1 (Specimen A)	Pullout force T_i (kN)	0.4	0.7	1.0	1.3	1.6	1.9	2.2	2.4	2.47
	Interface shear stress τ_i (kPa)	99.5	174.1	248.7	323.3	397.9	472.5	547.1	596.8	614.7
	T_i/UBS	0.16	0.28	0.40	0.53	0.65	0.77	0.89	0.97	
Specimen in Group 2 (Specimen B)	Pullout force T_i (kN)	0.2	0.3	0.4	0.45	0.5	0.55	0.6	0.65	0.68
	Interface shear stress τ_i (kPa)	49.7	74.6	99.5	111.9	124.3	136.8	149.2	161.6	168.4
	T_i/UBS	0.29	0.44	0.59	0.66	0.74	0.81	0.88	0.96	

will be represented by their short term as Specimen A and Specimen B.

It was assumed that the pullout force generates uniformly distributed shear stress over the entire interface bond area considering the design of this pullout setup (Chen *et al*. 2014, 2015). Hence, the interface shear stress corresponding to each loading level can be calculated by dividing the respective pullout force over interface bond area of the GFRP tendon, as

$$T_i = \tau_i d_n L \tag{1}$$

where T_i = pullout force of loading level i (i = 1 to 8 according to the adopted loading scheme shown in Table 3); τ_i = interface shear stress corresponding to the pullout force; d_n = nominal diameter of the GFRP tendon; and L = bond length of the GFRP tendon embedded in cemented soil. For the typical GFRP tendon used in this test, d_n is 16 mm and L is 80 mm.

Based on the experimental design, the tensile creep deformation of free GFRP tendons is insignificant compared with interface creep shear displacements. For instance, under the largest pullout load measured in this study (2.4 kN), the interface creep shear displacement was 1.568 mm at which the tensile elongation of the free GFRP tendon was only about 0.03 mm (1.9% of the interface creep shear displacement). In addition, the largest tensile stress on the free GFRP tendon measured in this study was 11.9 MPa, which was far less than its maximum tensile strength of 466 MPa (i.e. 2.6%), indicating that the tensile creep of the free GFRP tendon was negligible in this case.

Creep tests were carried out on the two pullout specimens with 180-day curing time using the creep pullout setup shown in Figures 2 and A3. Pullout specimens were sealed in the pullout cell with petroleum jelly to minimize moisture changes during creep tests. The laboratory temperature where the tests were conducted was maintained at 25 ± 2 degrees Celsius to minimize temperature effects on test results. Each loading level in the stepwise loading scheme was sustained until creep displacement change under this loading level was less than 0.01 mm in 24 h (Sun 1999).

4. EXPERIMENTAL RESULTS

The interface bond–slip curves obtained from the rapid pullout tests are shown in Figure 4. The peak bond stress

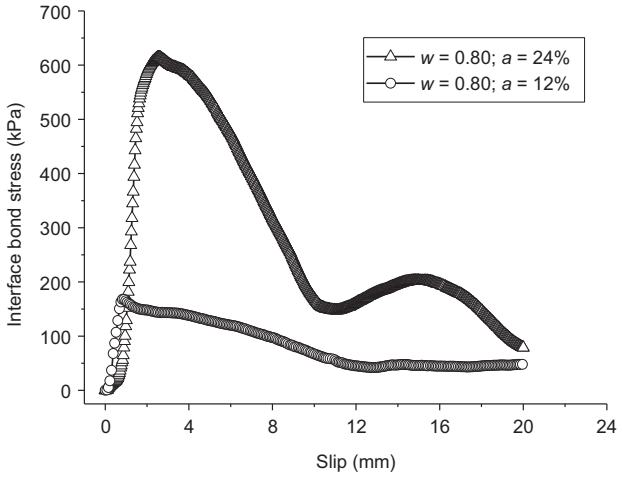

Figure 4. Interface bond–slip curves obtained in the rapid pullout tests

in the bond–slip curve (Figure 4) is defined as UBS; the magnitudes of UBS for the two rapid pullout specimens were 614.7 kPa (Specimen A with C_w = 0.80 and C_c = 24%) and 168.4 kPa (Specimen B with C_w = 0.80 and C_c = 12%).

The time histories of interface displacements obtained in the creep pullout test are presented in Figure 5, where the interface displacement is defined as the pullout displacement of the tendon head excluding the tensile deformation of the tendon's free segment. Tan's non-linear superposition method (Tan and Kang 1980) was adopted to transform the time history of interface displacements obtained in stepwise loading into a group of individual creep curves for the various loading levels. This superposition method accounts for the influence of creep rate under a given loading level or under the succeeding loading level, and the impact of loading history can be skillfully eliminated (Sun 1999; Lu *et al*. 2008; Zhang *et al*. 2010). Hence, the converted creep curves under various loading levels corresponded to independent stress states (i.e. free of loading history and coupling effect).

Figure 6 shows the creep curves under various loading levels for the two pullout specimens. It can be found that the creep curves corresponding to the first seven loading levels exhibited two creep phases, which can be defined as primary and steady. On the other hand, the creep curves corresponding to the ultimate loading level (i.e. eighth loading level) exhibited an additional tertiary creep phase.

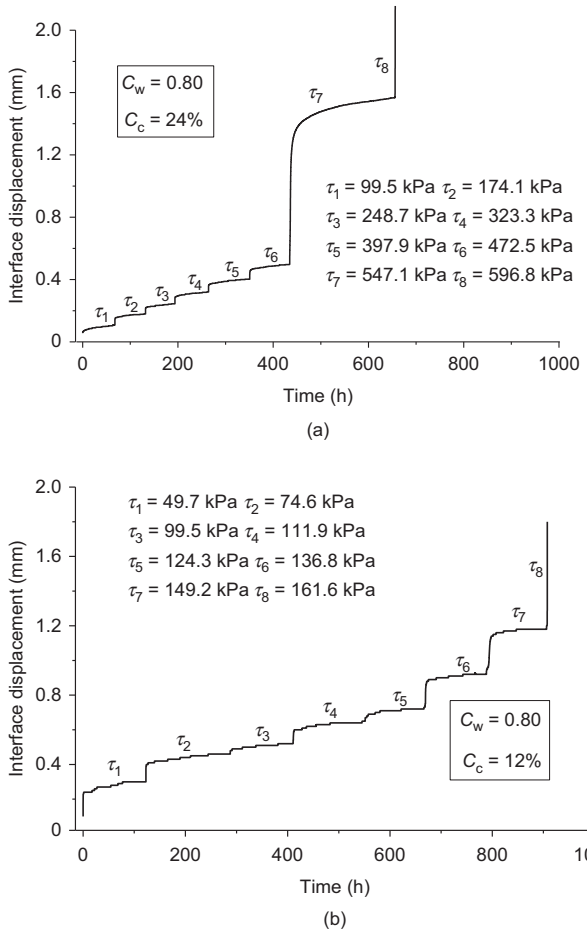

Figure 5. Time histories of interface displacements in creep pullout tests: (a) Specimen A; (b) Specimen B

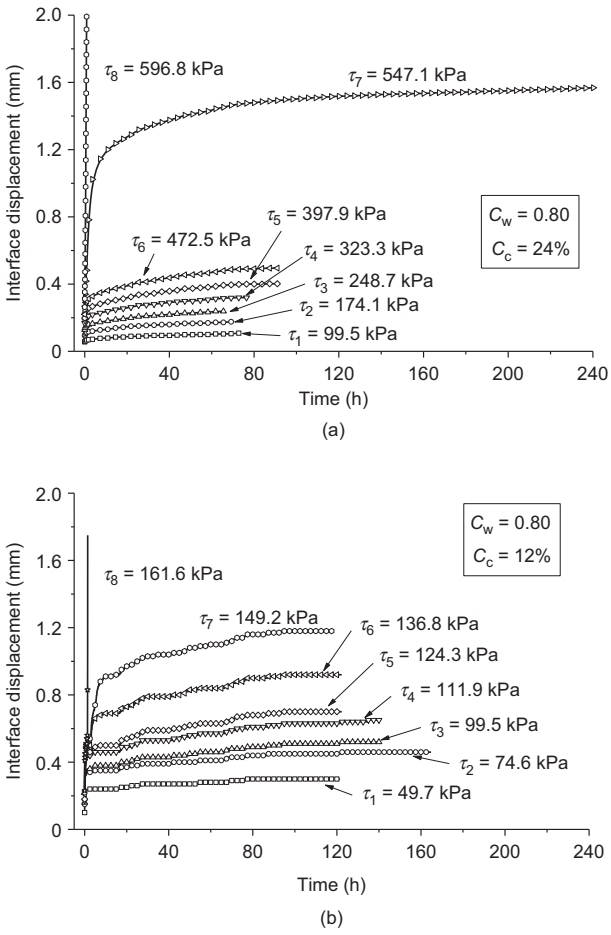

Figure 6. Creep curves under various loading levels: (a) Specimen A; (b) Specimen B

Similar observations were reported in literature (Kränkel *et al*. 2015; Cong and Hu 2017; Xu *et al*. 2018). The tertiary creep phase in the creep curve took place when the GFRP tendons were entirely pulled out from the encapsulating cemented soils. This indicates that creep pullout failure occurs under the loading level that first exhibits tertiary creep. The incremental creep displacements experienced by the two pullout specimens were compared under the same loading level (e.g. $\tau_1 = 99.5$ kPa for Specimen A and $\tau_3 = 99.5$ kPa for Specimen B). It was observed that Specimen A exhibited a smaller creep displacement than that of Specimen B (e.g. 0.11 mm for Specimen A versus 0.64 mm for Specimen B under $\tau = 99.5$ kPa). This indicates that the interface of Specimen A showed larger resistance to creep than that of Specimen B, which was attributed to the greater cement ratio of Specimen A compared with that of Specimen B.

5. INTERFACE CREEP MODELING OF GFRP TENDON IN CEMENTED SOILS

5.1. Modified Burgers model

As mentioned earlier, most of creep curves obtained from the creep pullout tests for GFRP tendons embedded in cemented soils (Figure 6) exhibited two creep phases, referred to herein as primary creep phase and steady creep phase. Tertiary creep phases were only observed in creep curves associated with the loading level corresponding to interface creep failure. Since it is very challenging to accurately obtain long-term interface shear strength from creep test results, rheological modeling was conducted as part of this study with the focus on creep behavior observed during the primary and steady phases. Burgers model (Cong and Hu 2017; Mansouri and Ajalloeian 2018) was modified by introducing a time-dependent viscosity element to characterize the creep behavior observed in this study. The schematic of the modified Burgers model is depicted in Figure 7.

As illustrated in Figure 7, the original Burgers model comprises a series connection by a Maxwell model (a spring and a dashpot connected in series) and a Kelvin model (a spring and a dashpot connected in parallel). The original Burgers model can be used to characterize the interface creep behavior presented in this study as

$$u = \frac{\tau}{G_1} + \frac{\tau}{\eta_1} t + \frac{\tau}{G_2}\left(1 - e^{-(G_2/\eta_2)t}\right) \tag{2}$$

where u = shear displacement of the GFRP tendon-cemented soil interface at a certain creep time; t = creep

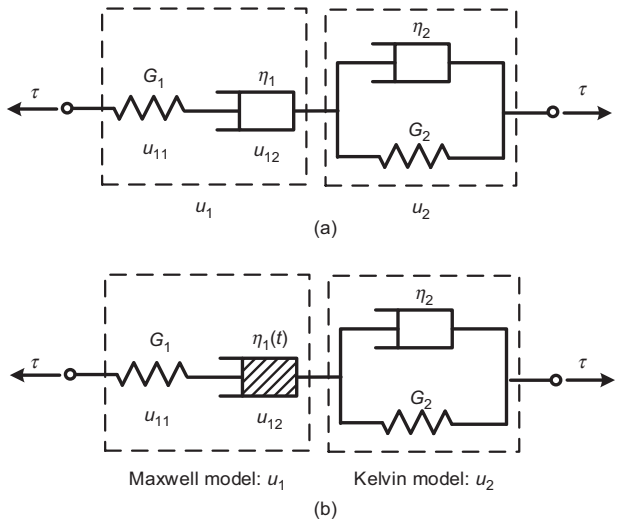

Figure 7. Schematic of two Burgers models: (a) the original Burgers model; (b) the modified Burgers model

time; τ = shear stress applied to the interface; G_1 and G_2 = spring shear moduli in Maxwell and Kelvin models, respectively; and η_1 and η_2 = dashpot viscosity coefficients in Maxwell and Kelvin models, respectively. The values of G_1 and G_2 depend on the initial and final creep displacements, respectively, under a given load; whereas, the values of η_1 and η_2 depend on the initial and final creep rates, respectively, under a given load (Behbahani *et al*. 2016; Cong and Hu 2017; Mansouri and Ajalloeian 2018).

It is noteworthy that the modeling was performed with respect to the converted creep curves (Figure 6) under respective loading levels, and this analysis of each creep curve under each single load was independent of and free of coupling with that under other loads. Hence, the time t used for each creep curve in modeling corresponds to the elapsed loading time of the current pullout load, rather than accumulated time of the past stepwise loading. In fact, the definition of time adopted in this work is fundamentally equal to the 'equivalent time' introduced by Yin and Graham (1989, 1994). In addition, the model parameters of the original Burgers model (G_1, η_1, G_2, and η_2) are constants. However, previous studies (Sun 1999; Chen *et al*. 2018a) reported that these parameters could vary with creep time and applied stress magnitude. The Burgers model was found to better characterize creep behavior for various materials when relevant model parameters were modified (Sun 1999; Cong and Hu 2017; Chen *et al*. 2018a). In this study, the viscosity coefficient was modified according to Sun (1999), where the change in creep rate obtained in this test was analyzed to facilitate the modification of viscosity coefficient. The creep rate was estimated as the slope of the creep curve as

$$\frac{du}{dt} = \frac{u_{i+1} - u_i}{\Delta t_{i,i+1}} \tag{3}$$

where u = interface displacement at a certain time t; and $\mathrm{d}u/\mathrm{d}t$ = creep rate at time t. The trend of the creep rate change over creep time for various creep curves obtained from the tests conducted in this study was interpreted using the aforementioned method (Tan and Kang 1980), as shown in Figure 8. As demonstrated for pullout Specimen A ($C_w = 0.80$ and $C_c = 24\%$), the creep rate in the primary creep phase (creep time less than 10 h) reduced with time for all curves under the various loading levels. It was observed that the curve corresponding to the ultimate creep loading level experienced some fluctuations, which could be attributed to the fact that a part of the interface area experienced bond failure and may have caused stick–slip behavior. The following equation was found to best fit the creep rate change with time (Figure 8):

$$\dot{u} = \frac{du}{dt} = \frac{\alpha}{\lambda^{t/t_0}}\tau \tag{4}$$

where $\dot{u}$ = creep rate; α and λ = dimensionless load-dependent fitting parameters; t_0 = reference creep time, which is set as one hour in this analysis as it is the time unit used throughout the test; and τ = shear stress applied to the interface.

By using the creep rate trend represented by Equation (4) to characterize the dashpot in the Maxwell

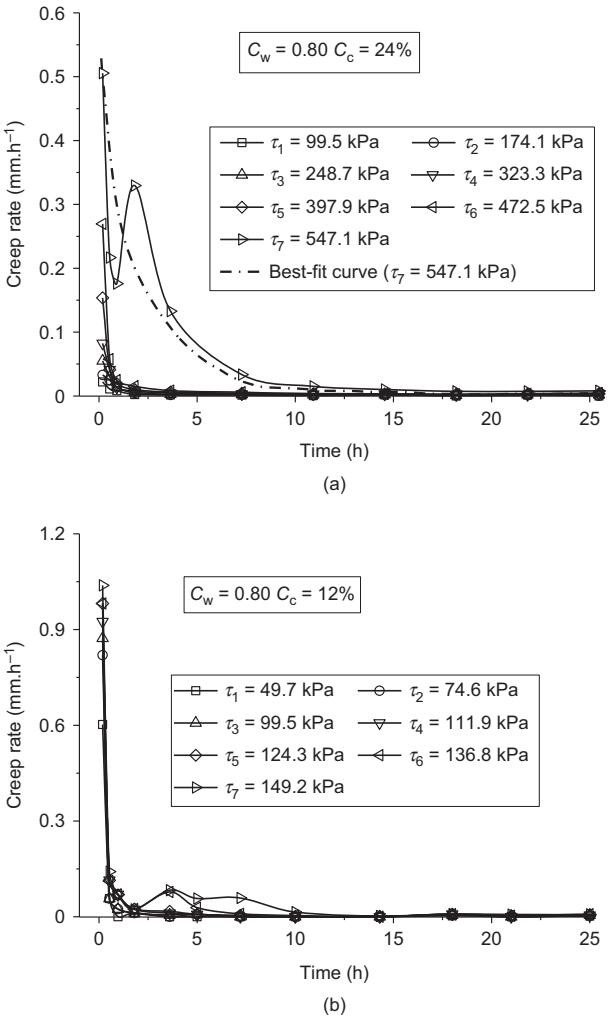

Figure 8. Variation of creep rate of pullout specimens over time: (a) Specimen A; (b) Specimen B

model ($\dot{u}_{12}$ in Figure 7)

$$\dot{u}_{12} = \frac{\tau}{\eta_1} = \frac{\alpha}{\lambda^{t/t_0}}\tau \tag{5}$$

Accordingly, the relationship between viscosity coefficient (η_1) and creep time (t) can be rewritten as

$$\eta_1 = \eta_1(t) = \frac{\lambda^{t/t_0}}{\alpha} \tag{6}$$

Defining $\eta_0 = 1/\alpha$ results in

$$\begin{cases} \dot{u}_{12} = \dfrac{\tau}{\eta_1(t)} \\ \eta_1(t) = \eta_0 \cdot \lambda^{t/t_0} \end{cases} \tag{7}$$

where η_0 = dashpot viscosity coefficient in the Maxwell model at the initial creep time ($t \to 0$); and λ = nonlinear attenuation coefficient of $\eta_1(t)$. Note that the value of λ increases with the increasing rate of the viscosity coefficient (η_1). The value of $\lambda = 1$ corresponds to the dashpot in the Maxwell model with the linear attenuation for the viscosity coefficient.

Creep displacement of the dashpot in the Maxwell model ($u_{12}(t)$) can be obtained by integrating Equation (7) and using the boundary condition $u_{12} = 0$ at $t = 0$ to solve the integration constant as

$$u_{12} = \frac{\tau}{\eta_0}\left(\frac{t_0}{\ln\lambda} - \frac{t_0\lambda^{-t/t_0}}{\ln\lambda}\right) \tag{8}$$

By replacing the linear dashpot in the Maxwell model with the developed nonlinear dashpot, the modified nonlinear Burgers model could be established (Figure 7) as

$$u = u_1 + u_2 = \frac{\tau}{G_1} + \frac{\tau}{\eta_0}\left(\frac{t_0}{\ln\lambda} - \frac{t_0\lambda^{-t/t_0}}{\ln\lambda}\right) + \frac{\tau}{G_2}(1 - e^{-(G_2/\eta_2)t}) \tag{9}$$

where G_1, η_0, G_2, η_2, and λ = five parameters of the modified nonlinear Burgers model, of which the values can be determined based on the obtained test results.

5.2. Interface shear creep model of GFRP tendon embedded in cemented soils

The estimation is the application of the interface shear creep model in practice by interpolating (extrapolation is not suggested to avoid the interface creep failure) the relationship between the model parameter and interface shear stress. Because the limited number of testing levels of interface shear stress (discrete variable) can be adopted in the laboratory test, the actual interface shear stress applied to the interface in practice is very probably located within the tested range, but this is not the same with the adopted ones in testing. The interpolation of the relationship is essentially the necessary counterpart of developing the interface creep model as presented in the work.

To complete the abovementioned framework of applicability of the modeling, the testing data were deliberately divided into regression set (within the testing range, e.g. τ_1, τ_3, τ_5, and τ_7 for Specimen A) and verification set (within the testing range, e.g. τ_2, τ_4, and τ_6 for Specimen A), as shown in Figure 6.

Table 4. Values of parameters of interface shear creep model obtained in fittings for regression set

τ (kPa)	G_1 (kPa)	η_0 (kPa·h)	λ	G_2 (kPa)	η_2 (kPa·h)	R^2 [a]
Specimen A						
99.5	1758.5	5959.9	3.53	2377.0	95081.3	0.992
248.7	1925.8	4040.4	9.55	2531.4	95705.6	0.998
397.9	1991.3	2647.6	18.93	2339.6	90152.0	0.998
547.1	2308.6	1361.6	1.56	1303.9	62954.9	0.998
Specimen B						
49.7	463.8	112.8	33.11	555.4	31738.8	0.951
99.5	537.9	232.1	11.26	468.1	33721.8	0.960
124.3	522.4	301.5	5.12	400.7	30593.4	0.976
149.2	471.9	379.5	2.10	317.5	24719.3	0.969

[a]Note: R^2 is the coefficient of correlation.

The procedure of establishing the interface creep model was demonstrated based on the test results of Specimen A (water content $C_w = 0.80$; cement content $C_c = 24\%$) as follows:

- Step 1: Creep curves in the regression set were fitted using the modified Burgers model (Equation (9)). The values of model parameters were derived in the fitting as listed in Table 4, and the fitting effectiveness was presented by solid lines in Figure 9(a).
- Step 2: Correlations of model parameters of the interface shear creep model (G_1, η_0, G_2, η_2, and λ) and the interface shear stress were fitted using exponential or polynomial functions, respectively. The fitting functions and the fitting effectiveness for Specimen A were presented in Figure 10 and Equation (10).
- Step 3: By substituting the determined values of model parameters into the modified Burgers model (Equation (9)), the interface shear creep model for the GFRP tendon embedded in cemented soils, specifically for Specimen A ($C_w = 0.80$ and $C_c = 24\%$), can be rewritten as

$$u = \frac{\tau}{G_1} + \frac{\tau}{\eta_0}\left(\frac{t_0}{\ln\lambda} - \frac{t_0\lambda^{-t}}{\ln\lambda}\right) + \frac{\tau}{G_2}(1 - e^{-(G_2/\eta_2)t}) \tag{10a}$$

$$G_1 = 1665.4 + 81.3 \times e^{0.0038\tau} \tag{10b}$$

$$\eta_0 = -3657.0 + 11082.0 \times e^{-0.0014\tau} \tag{10c}$$

$$\lambda = -0.25 - (0.5 \times \tau - 276.3) \times e^{0.0091\tau - 5.0} \tag{10d}$$

$$G_2 = 2452.4 - 0.15 \times e^{0.0164\tau} \tag{10e}$$

$$\eta_2 = 95823.4 - 45.4 \times e^{0.012\tau} \tag{10f}$$

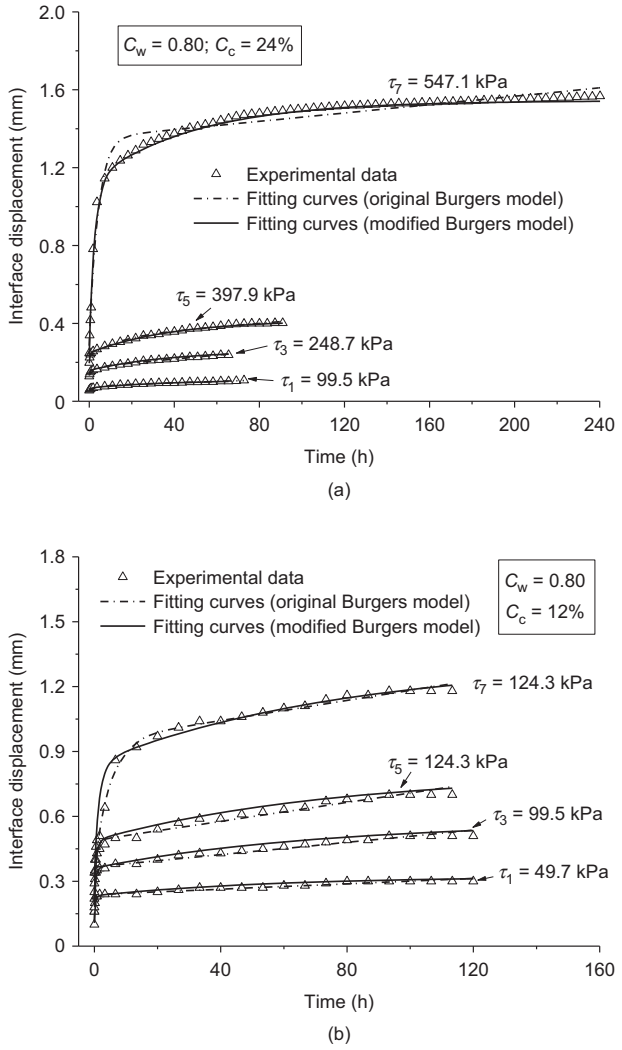

Figure 9. Fittings on creep curves in regression set using original and modified Burgers models: (a) Specimen A; (b) Specimen B

The interface shear creep model for Specimen B ($C_w = 0.80$ and $C_c = 12\%$) was also obtained using the same procedure as

$$u = \frac{\tau}{G_1} + \frac{\tau}{\eta_0}\left(\frac{t_0}{\ln\lambda} - \frac{t_0\lambda^{-t}}{\ln\lambda}\right) + \frac{\tau}{G_2}(1 - e^{-(G_2/\eta_2)t}) \quad (11a)$$

$$G_1 = -0.028 \times \tau^2 + 5.71 \times \tau + 249.8 \quad (11b)$$

$$\eta_0 = 0.0058 \times \tau^2 + 1.53 \times \tau + 22.5 \quad (11c)$$

$$\lambda = 0.00256 \times \tau^2 - 0.821 \times \tau + 67.6 \quad (11d)$$

$$G_2 = -0.00128 \times \tau^2 + 0.154 \times \tau + 579.4 \quad (11e)$$

$$\eta_2 = -2.221 \times \tau^2 + 371.2 \times \tau + 18769 \quad (11f)$$

Note that the polynomial functions used in correlating the model parameters with the interface shear stress for Specimen B were chosen to achieve the best fitting effectiveness.

The corresponding regression parameters of the original Burgers model for the creep curves in regression set were determined using a similar technique, as shown in Table 5. Figure 9 shows a comparison between the creep displacements measured experimentally and those fitted using both the original and the modified Burgers models. Figures 9(a) and 9(b) shows the creep curves corresponding to interface shear stresses of τ_1, τ_3, τ_5, and τ_7 for pullout Specimen A and B, respectively. Good agreement was observed between the fitted and measured values at relatively low interface shear stresses (τ_1, τ_3, and τ_5) for both the preceding models. However, it was observed that the fitting curves of the modified Burgers model demonstrated better agreement with the measured data at a relatively higher interface shear stress (τ_7).

5.3. Predicting capability of the interface shear creep model

The concept of prediction used in this context can be more accurately defined as the verification of estimations using the developed regression model. The fitting effectiveness of the interface shear creep model was demonstrated in the precedent subsection using test results in the regression set. The predicting capability of the interface creep model was evaluated using test results in the verification set in the following steps: (a) substitute the values of interface shear stress in the verification set (τ_2, τ_4, and τ_6) into the correlations Equations (10) and (11) to determine the model parameters under respective interface shear stress for two pullout specimens as listed in Table 6; (b) compare the predicted creep curves based on the determined interface creep model with the creep curves measured in pullout creep tests as shown in Figure 11; (c) determine the corresponding parameters in original Burgers model for the creep curves in the verification set using a similar technique as in step (a), as presented in Table 7; and (d) compare the predicted curves derived in the presented interface shear creep model and in the original Burgers model as shown in Figure 11.

The applicability of the presented interface shear creep model (modified Burgers model) was substantially validated by the predicting accuracy and effectiveness of the measured creep curves. The presented creep model was observed to exhibit higher predicting capability than that of the original Burgers model by manifesting a much smaller offset between the trends in measured and predicted creep curves. This predicting superiority was more obviously observed for creep curves under higher interface shear stress (τ_6). This is because the nonlinearity of interface creep increases with the applied shear stress level, especially when the applied interface shear stress approaches the long-term interface strength. The modified Burgers model exceeded the original Burgers model in characterizing nonlinear creep behavior by introducing an improved dashpot with time-dependent viscosity coefficient as described preciously. In addition, as suggested in Figure 10, the values of model parameters tend to change remarkably over a higher interface shear stress range (exponential or polynomial change), which means a slight bias between the applied and the measured shear stress could induce substantial difference of the model parameters. The good agreement between the

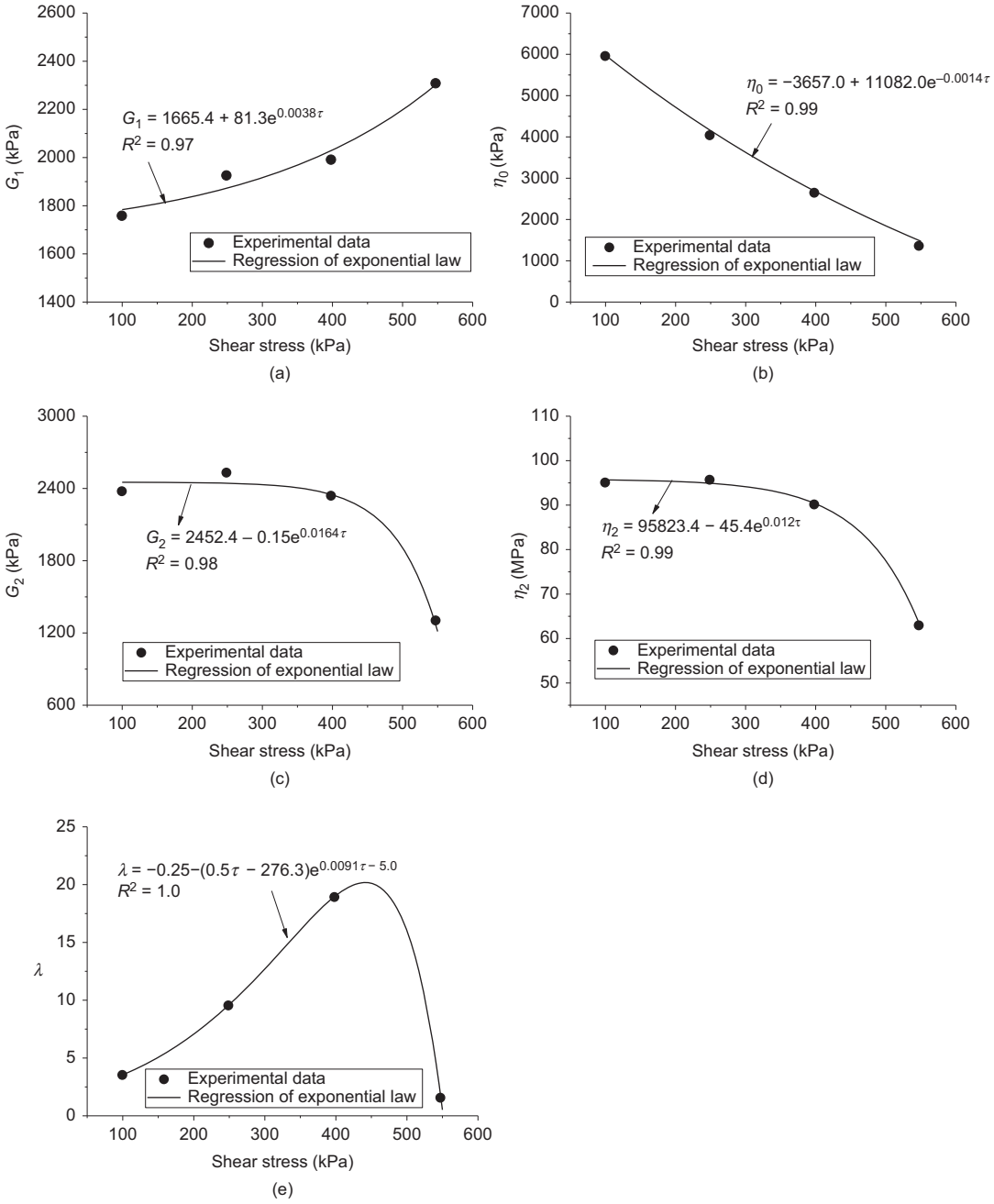

Figure 10. Correlations of model parameters and interface shear stress obtained in fitting for Specimen A: (a) G_1; (b) η_0; (c) G_2; (d) η_2; (e) λ

Table 5. Values of parameters of original Burgers model obtained in fittings for regression set

τ (kPa)	G_1 (kPa)	η_1 (kPa·h)	G_2 (kPa)	η_2 (kPa·h)	R^2
Specimen A					
99.5	1655.2	24580.1	4869.4	275670.1	0.988
248.7	1814.1	18044.9	6389.9	243132.9	0.986
397.9	1734.9	53096.0	3953.1	451306.3	0.982
547.1	1917.5	1955.1	512.8	509560.4	0.981
Specimen B					
49.7	413.5	53.8	420.5	79922.9	0.964
99.5	518.5	78.4	569.6	70214.4	0.969
124.3	517.3	240.5	498.5	56921.0	0.970
149.2	449.7	1036.8	241.5	63983.5	0.952

Table 6. Values of parameters of interface shear creep model obtained in prediction for verification set

τ (kPa)	G_1 (kPa)	η_0 (kPa·h)	λ	G_2 (kPa)	η_2 (kPa·h)	R^2
Specimen A						
174.1	1821.8	4967.6	5.96	2449.9	95454.3	0.996
323.3	1939.3	3300.0	14.26	2423.3	93599.2	0.998
472.5	2145.3	1954.9	19.07	2114.6	82425.4	0.997
Specimen B						
74.6	518.3	168.8	20.6	519.6	34103.5	0.968
111.9	534.5	266.0	7.8	436.4	32501.5	0.981
136.8	501.5	339.8	3.2	361.1	27999.1	0.978

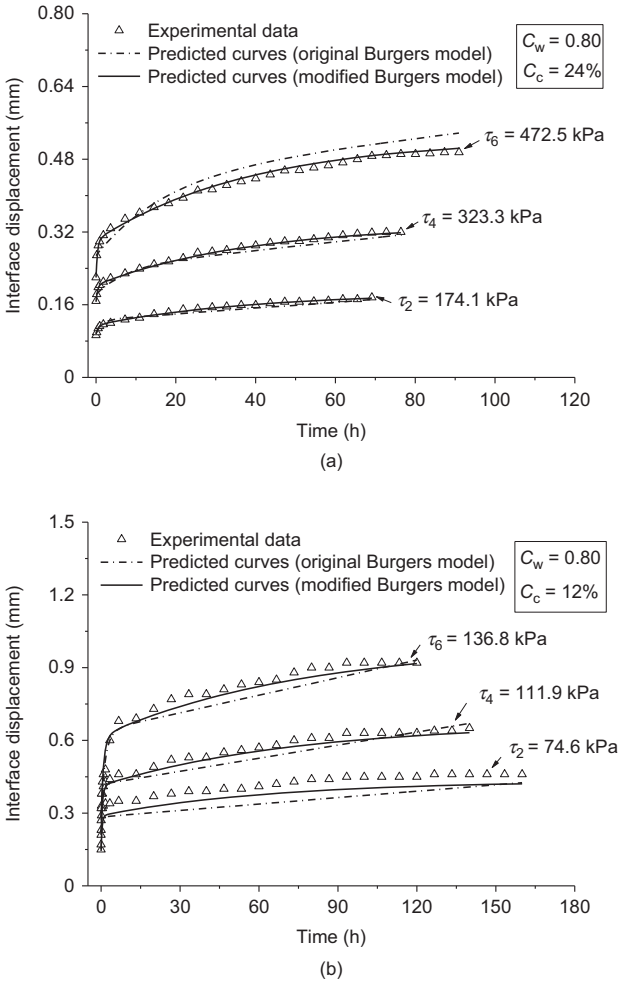

Figure 11. Predictions on creep curves in verification set using both original and modified Burgers models: (a) Specimen A; (b) Specimen B

Table 7. Values of parameters of original Burgers model obtained in prediction for verification set

τ (kPa)	G_1 (kPa)	η_1 (kPa·h)	G_2 (kPa)	η_2 (kPa·h)	R^2
Specimen A					
174.1	1795.7	8128.0	5791.9	273258.6	0.978
323.3	1773.0	38358.3	5481.3	341545.1	0.985
472.5	1762.2	46285.7	2690.3	455227.4	0.971
Specimen B					
74.6	490.8	149.9	563.8	84353.7	0.946
111.9	522.7	105.7	547.2	62160.7	0.952
136.8	487.1	535.2	379.6	56542.2	0.974

predicted and the measured creep curves also validated the accuracy of the presented correlations relating model parameters and interface shear stress.

6. CONCLUSIONS

Interface creep behavior of GFRP tendons embedded in cemented soils was investigated using element pullout creep tests in this work. A set of specimen preparation devices and a pullout setup were specially designed and used to prepare element pullout specimen with different cement–moisture contents of cemented soils and implement stepwise creep loading on pullout specimens. A novel interface shear creep model was developed to characterize the creep behavior of the interface between GFRP tendons and cemented soils by implementing regression analysis on test results. Findings and concluded remarks obtained in this work are presented as follows:

- The presented specially designed pullout creep test setup based on element pullout specimens is applicable to test the interface creep behavior of GFRP tendons embedded in cemented soils with cement–moisture content conditioned.
- The stepwise loading strategy for pullout creep test should be determined from a rapid pullout test for parallel pullout specimens to ensure the maximum interface shear stress applied in the creep test is less than the UBS obtained in the rapid pullout test.
- Both interface shear and interface creep responses of GFRP tendons embedded in cemented soils were largely impacted by the cement and moisture contents of the cemented soils where the tendons were embedded.
- Burgers model modified by introducing dashpot element with time-dependent viscosity coefficient calibrated using creep pullout test results can be used to characterize the interface creep behavior of GFRP tendons embedded in cemented soils under different interface shear stresses that did not induce the occurrence of the tertiary creep phase.

Overall, this study presented adequate means of in-laboratory interface creep characterization of GFRP tendons embedded in cemented soils and provided insights into the time-dependent reinforcement-matrix interface strength mobilization and long-term work performance of soil-mixing structures reinforced by GFRP tendons.

ACKNOWLEDGMENTS

This work was sponsored by the National Natural Science Foundation of China (Grant Nos. 51978254, 51908201, and 41572298), the State Administration of Foreign Experts Affairs of China (Grant No. G20190018010), the Natural Science Foundation of Hunan Province (Grant No. 2020JJ5024), the Science and Technology Program of Changsha (grants number: kq2004013), and Hunan Provincial Innovation Foundation for Postgraduate (grants number: CX20210410). The authors appreciate their support.

NOTATION

Basic SI units are given in parentheses.

C_c cement content of cemented soil specimens (dimensionless)
C_u coefficient of uniformity (dimensionless)

C_w water content of cemented soil specimens (dimensionless)
C_z coefficient of curvature (dimensionless)
c_u undrained shear strength (Pa)
d_n nominal diameter of GFRP tendon (m)
E elasticity modulus of GFRP tendon (Pa)
e void ratio of soil (dimensionless)
G_1 spring shear moduli in Maxwell models (Pa)
G_2 spring shear moduli in Kelvin models (Pa)
G_s specific gravity (dimensionless)
I_p plasticity index (dimensionless)
L bond length of the GFRP tendon embedded in cemented soil (m)
R_h rib height of GFRP tendon (m)
R_s rib spacing of GFRP tendon (m)
T_i pullout force of loading level i ($i = 1$ to 8 according to the adopted loading scheme shown in Table 3) (N)
t creep time (s)
t_0 reference creep time, which is set as one hour in this analysis as it is the time unit used throughout the test (s)
u shear displacement of the GFRP tendon-cemented soil interface (m)
$\dot{u}$ creep rate (m/s)
w natural water content of soil (dimensionless)
w_l liquid limit (dimensionless)
w_p plastic limit (dimensionless)
α load-dependent fitting parameters (dimensionless)
η_0 dashpot viscosity coefficient in Maxwell model at the initial creep time ($t \rightarrow 0$) (Pa·s)
η_1 dashpot viscosity coefficients in Maxwell models (Pa·s)
η_2 dashpot viscosity coefficients in Kelvin models (Pa·s)
λ nonlinear attenuation coefficient of $\eta_1(t)$ (dimensionless)
ρ bulk density of soil (kg/m^3)
σ_b tensile strength of GFRP tendon (Pa)
τ_i interface shear stress corresponding to the pullout force (Pa)

ABBREVIATIONS

DMW deep mixing walls
FRP fiber-reinforced polymer
GFRP glass fiber-reinforced polymer
UBS ultimate interface bond strength

REFERENCES

ACI (2015). *440.1R: Guide for the Design and Construction of Structural Concrete Reinforced with FRP Bars*. ACI Committee 440, American Concrete Institute, Farmington Hills, MI, USA.

Alves, J., El-Ragaby, A. & El-Salakawy, E. (2011). Durability of GFRP bars bond to concrete under different loading and environmental conditions. *Journal of Composites for Construction*, **15**, No. 3, 249–262.

Ascione, L., Berardi, V. P. & D'Aponte, A. (2012). Creep phenomena in FRP materials. *Mechanics Research Communications*, **43**, 15–21.

Bai, X. Y., Zhang, M. Y. & Zhang, S. Q. (2015). Creep testing on anti-floating anchors of full-length bonding thread glass fiber reinforced polymer (GFRP). *Chinese Journal of Rock Mechanics and Engineering*, **34**, No. 4, 804–813 (in Chinese).

Bakeer, R. M., Sayed, S. M., Cates, P. & Subramanian, R. (1998). Pullout and shear tests on geogrid reinforced lightweight aggregate. *Geotextiles & Geomembranes*, **16**, No. 2, 119–133.

Behbahani, H., Ziari, H. & Kamboozia, N. (2016). Evaluation of the visco-elasto-plastic behavior of glasphalt mixtures through generalized and classic Burger's models modification. *Construction and Building Materials*, **118**, 36–42.

Benmokrane, B., Chennouf, A. & Mitri, H. S. (1995). Laboratory evaluation of cement-based grouts and grouted rock anchors. *International Journal of Rock Mechanics and Mining Sciences*, **32**, No. 7, 633–642.

Benmokrane, B., Xu, H. X. & Bellavance, E. (1996). Bond strength of cement grouted glass fibre reinforced plastic (GFRP) anchor bolts. *International Journal of Rock Mechanics and Mining Science & Geomechanics*, **33**, No. 5, 455–465.

CECS (2016). *147: Technical Specification for Soil Mass with reinforced cement soil pile and anchors*. China Planning Press, Beijing, China (in Chinese).

Cheng, Y. M., Choi, Y. K., Yeung, A. T., Tham, L. G., Alfred, S. K., Wei, W. B. & Chen, J. (2009). New soil nail material – pilot study of grouted GFRP pipe nails in Korea and Hong Kong. *Journal of Materials in Civil Engineering*, **21**, No. 3, 93–102.

Chen, C. F., Gao, J., Liu, J. B. & Huang, M. H. (2018a). A factional-derivative-based creep model for the soil-anchor interface in the anchored slope with the soil expanding. *Journal of Safety and Environment*, **18**, No. 5, 1847–1854 (in Chinese).

Chen, C. F., Huang, J. B., Zhang, G. B. & Zhu, S. M. (2019a). Bond behavior of tensioned GFRP tendons embedded in cemented soils. *Journal of Tianjin University (Science and Technology)*, **52**, No. S1, 120–127 (in Chinese).

Chen, C. F., Liang, G. T., Tang, Y. & Xu, Y. L. (2015). Anchoring solid-soil interface behavior using a novel laboratory testing technique. *Chinese Journal of Geotechnical Engineering*, **37**, No. 6, 1115–1122 (in Chinese).

Chen, C. F., Liang, G. T., Zhang, G. B., Tang, Y., Zheng, X. X., Sun, Y., Wang, S. Y. & Wang, C. Z. (2014). *A device and method for preparing soil samples used in testing frictional performance of anchor/pile-soil interface*. China Patent ZL 2014 1 0176979.8, filed April 29, 2014, and issued July 6, 2016.

Chen, C. F., Liu, J. B., Xu, Y. L. & Zhang, G. B. (2016). Tests on shearing creep of anchor-soil interface and its empirical model. *Chinese Journal of Geotechnical Engineering*, **38**, No. 10, 1762–1768 (in Chinese).

Chen, C. F., Zhang, G. B., Zornberg, J. G., Morsy, A. M. & Huang, J. B. (2020). Interface bond behavior of tensioned glass fiber-reinforced polymer (GFRP) tendons embedded in cemented soils. *Construction and Building Materials*, **263**, 120132.

Chen, C. F., Zhang, G. B., Zornberg, J. G., Morsy, A. M., Zhu, S. M. & Zhao, H. B. (2018b). Interface behavior of tensioned bars embedded in cement-soil mixtures. *Construction and Building Materials*, **186**, 840–853.

Chen, C. F., Zhang, G. B., Zornberg, J. G. & Zheng, X. X. (2019b). Element nail pullout tests for prediction of soil nail pullout resistance in expansive clays. *Geotechnical Testing Journal*, **42**, No. 5, 1274–1297.

Chen, C. F., Zhu, S. M., Gao, J., Wen, Y. K. & Mao, F. S. (2019c). Kriging method-based creep model for anchor-soil interface considering grouting pressure. *Chinese Journal of Geotechnical Engineering*, **41**, No. S1, 125–128 (in Chinese).

Chu, L. M. & Yin, J. H. (2005). Comparison of interface shear strength of soil nails measured by both direct shear box tests and pullout tests. *Journal of Geotechnical and Geoenvironmental Engineering*, **131**, No. 9, 1097–1107.

Cong, L. & Hu, X. L. (2017). Triaxial rheological property of sandstone under low confining pressure. *Engineering Geology*, **231**, 45–55.

Consoli, N. C., Rosa, D. A., Cruz, R. C. & Rosa, A. D. (2011). Water content, porosity and cement content as parameters controlling

strength of artificially cemented silty clay. *Engineering Geology*, **122**, 328–333.

Cooke, R. W., Price, G. & Tarr, K. (1979). Jacked piles in London Clay: A study of load transfer and settlement under working conditions. *Géotechnique*, **29**, No. 2, 113–147.

Frost, J. D. & Han, J. (1999). Behavior of interfaces between fiber-reinforced polymers and sands. *Journal of Geotechnical and Geoenvironmental Engineering*, **125**, No. 8, 633–640.

Gao, J., Zhu, S. M. & Chen, C. F. (2018). RBF Neural network based creep model of red clay-anchor interface. *Chinese Journal of Geotechnical Engineering*, **40**, No. S2, 122–126 (in Chinese).

Guades, E., Aravinthan, T., Islam, M. & Manalo, A. (2012). A review on the driving performance of FRP composite piles. *Composite Structures*, **94**, No. 6, 1932–1942.

Iskander, M. G., Hanna, S. & Stachula, A. (2001). Driveability of FRP composite piling. *Journal of Geotechnical and Geoenvironmental Engineering*, **127**, No. 2, 169–176.

Jamsawang, P., Bergado, D., Bandari, A. & Voottipruex, P. (2008). Investigation and simulation of behavior of stiffened deep cement mixing (SDCM) piles. *International Journal of Geotechnical Engineering*, **2**, No. 3, 229–246.

JGJ/T (2011). *233: Specification for Mix Proportion Design of Cement Soil*. Architecture and Building Press, Beijing, China (in Chinese).

Kim, K. H. E. & Andrawes, B. (2016). Compression behavior of FRP strengthened bridge timber piles subjected to accelerated aging. *Construction & Building Materials*, **124**, 177–185.

Kou, H. L., Guo, W. & Zhang, M. Y. (2015). Pullout performance of GFRP anti-floating anchor in weathered soil. *Tunnelling and Underground Space Technology*, **49**, 408–416.

Koupouli, N. J. F., Belem, T., Rivard, P. & Effenguet, H. (2016). Direct shear tests on cemented paste backfill-rock wall and cemented paste backfill-backfill interfaces. *Journal of Rock Mechanics and Geotechnical Engineering*, **8**, 472–479.

Kränkel, T., Lowke, D. & Gehlen, C. (2015). Prediction of the creep behaviour of bonded anchors until failure - a rheological approach. *Construction and Building Materials*, **75**, 458–464.

Liu, F. Y., Wang, P., Geng, X., Wang, J. & Lin, X. (2016). Cyclic and post-cyclic behavior from sand-geogrid interface large-scale direct shear tests. *Geosynthetics International*, **23**, No. 2, 129–139.

Liu, Z. B., Xie, S. Y., Shao, J. F. & Conil, N. (2018). Multi-step triaxial compressive creep behaviour and induced gas permeability change of clay-rich rock. *Géotechnique*, **68**, No. 4, 281–289.

Liu, G. B., Ye, R. H., Shen, X. Y. & Shen, C. L. (2010). Mechanism of cement-soil mixing anchor and application in foundation pit support project. *Chinese Journal of Geotechnical Engineering*, **32**, No. S2, 363–366 (in Chinese).

Lu, P. Z., Zeng, J. & Sheng, Q. (2008). Creep tests on soft clay and its empirical models. *Rock and Soil Mechanics*, **29**, No. 4, 1041–1044 (in Chinese).

Mansouri, H. & Ajalloeian, R. (2018). Mechanical behavior of salt rock under uniaxial compression and creep tests. *International Journal of Rock Mechanics and Mining Sciences*, **110**, 19–27.

Mirmiran, A., Shao, Y. & Shahawy, M. (2002). Analysis and field tests on the performance of composite tubes under pile driving impact. *Composite Structures*, **55**, No. 2, 127–135.

Mukhtar, F. M. & Faysal, R. M. (2018). A review of test methods for studying the FRP-concrete interfacial bond behavior. *Construction & Building Materials*, **169**, 877–887.

Najafabadi, E. P., Bazli, M., Ashrafi, H. & Oskouei, A. V. (2018). Effect of applied stress and bar characteristics on the short-term creep behavior of FRP bars. *Construction & Building Materials*, **171**, 960–968.

Nasir, O. & Fall, M. (2008). Shear behaviour of cemented pastefill-rock interfaces. *Engineering Geology*, **101**, 146–153.

Sakr, M., El Naggar, M. H. & Nehdi, M. (2004). Load transfer of fibre-reinforced polymer (FRP) composite tapered piles in dense sand. *Canadian Geotechnical Journal*, **41**, No. 1, 70–88.

Sheikh, S. A. & Kharal, Z. (2018). Replacement of steel with GFRP for sustainable reinforced concrete. *Construction and Building Materials*, **160**, 767–774.

Shina, K., Okubob, S., Fukui, K. & Hashiba, K. (2005). Variation in strength and creep life of six Japanese rocks. *International Journal of Rock Mechanics & Mining Sciences*, **42**, 251–260.

Sun, J. (1999). *Rheological behavior of geomaterials and its engineering applications*, China Architecture and Building Press, Beijing, China, pp. 61–62 (in Chinese).

Tan, T. K. & Kang, W. F. (1980). Locked in stresses, creep and dilatancy of rocks, and constitutive equations. *Rock Mechanics*, **13**, No. 1, 5–22.

Wang, J., Cai, Y. & Huang, D. Y. (2004). Testing research on thermal creep strain model of prestressing tendons and application of FEM analysis. *China Civil Engineering Journal*, **37**, No. 11, 1–6 (in Chinese).

Xu, D. S. & Yin, J. H. (2016). Analysis of excavation induced stress distributions of GFRP anchors in a soil slope using distributed fiber optic sensors. *Engineering Geology*, **213**, 55–63.

Xu, M., Jin, D. H., Song, E. X. & Shen, D. W. (2018). A rheological model to simulate the shear creep behavior of rockfills considering the influence of stress states. *Acta Geotechnica*, **13**, 1313–1327.

Yin, J. H. & Graham, J. (1989). Visco-elastic-plastic modelling of one-dimensional time-dependent behaviour of clays. *Canadian Geotechnical Journal*, **26**, 199–209.

Yin, J. H. & Graham, J. (1994). Equivalent times and one-dimensional elastic visco-plastic modeling of time-dependent stress-strain behavior of clays. *Canadian Geotechnical Journal*, **31**, 42–52.

Zemour, N., Asadian, A., Ahmed, E. A., Khayat, K. H. & Benmokrane, B. (2018). Experimental study on the bond behavior of GFRP bars in normal and self-consolidating concrete. *Construction & Building Materials*, **189**, 869–881.

Zhang, G. B., Chen, C. F., Zornberg, J. G., Morsy, A. M. & Mao, F. S. (2020). Interface creep behavior of grouted anchors in clayey soils: Effect of soil moisture condition. *Acta Geotechnica*, **15**, 2159–2177.

Zhang, X. W., Wang, C. M. & Zhang, S. H. (2010). Comparative analysis of soft clay creep data processing method. *Journal of Jilin University (Earth Science Edition)*, **40**, No. 6, 1401–1408, (in Chinese).

Zhang, C. C., Zhu, H. H., Shi, B., Wu, F. D. & Yin, J. H. (2015). Experimental investigation of pullout behavior of fiber-reinforced polymer reinforcements in sand. *Journal of Composites for Construction*, **19**, No. 3, 04014062.

Zheng, J. J. & Dai, J. G. (2014a). Analytical solution for the full-range pull-out behavior of FRP ground anchors. *Construction and Building Materials*, **58**, 129–137.

Zheng, J. J. & Dai, J. G. (2014b). Prediction of the nonlinear pull-out response of FRP ground anchors using an analytical transfer matrix method. *Engineering Structures*, **81**, 377–385.

Zhu, H. H., Yin, J. H., Yeung, A. T. & Jin, W. (2011). Field pullout testing and performance evaluation of GFRP soil nails. *Journal of Geotechnical and Geoenvironmental Engineering*, **137**, No. 7, 633–642.

The Editor welcomes discussion on all papers published in Geosynthetics International. Please email your contribution to discussion@geosynthetics-international.com by 15 December 2022.